Materials Today: Proceedings 62 (2022) 1521–1525

Contents lists available at ScienceDirect

Materials Today: Proceedings

journal homepage: www.elsevier.com/locate/matpr

# Design and simulation of 6-DOF cylindrical robotic manipulator using finite element analysis

Atirav Seth [a,*], Jordan Kurian Kuruvilla [a], Shashwat Sharma [b], Jyotishka Duttagupta [b], Ankur Jaiswal [a]

[a] Department of Mechatronics, Manipal Institute of Technology, Manipal Academy of Higher Education (MAHE), Manipal, Karnataka 576104, India
[b] Department of Mechanical Engineering, Manipal Institute of Technology, Manipal Academy of Higher Education (MAHE), Manipal, Karnataka 576104, India

ARTICLE INFO

*Article history:*
Available online 3 March 2022

*Keywords:*
6-DOF Cylindrical Manipulator
FEM
CAD Modeling
Leadscrew actuation mechanism
Timing belt actuation
Non-back drivable revolute joint
Space frame assembly

ABSTRACT

One of the several applications of robotic manipulators is aiding Unmanned Ground Vehicles (UGVs) in performing dexterous tasks. They have a variety of applications, from gathering rocks or soil samples to being employed as military UGVs. Robotic manipulators for these applications must be able to withstand high inertial loads that might be incurred during cases such as collisions at high speeds or traversal over rugged terrain. This study provides a 6 Degree of Freedom cylindrical manipulator designed according to the suitable parameters. This demands that the manipulator be structurally sound while minimizing weight to maintain a balanced center of gravity. The manipulator can be divided into the 3-DOF cylindrical arm with a prismatic-revolute-prismatic configuration and a 3- DOF end effector. Hollow tubes and plates with truss patterns are utilized to maximize the stiffness to weight ratio. Materials with a high strength-to-weight ratio such as carbon fiber and aluminum alloy (6061-T6 and 7075-T6) are used. The system has a non-back drivable actuation and can lift up to 5 Kgs while sustaining all the challenging circumstances encountered during extreme traversal. SOLIDWORKS was used to create the CAD model, while ANSYS workbench was used for structural analysis.

Selection and peer-review under responsibility of the scientific committee of the International Conference on Recent Advances in Modeling and Simulations Techniques in Engineering and Science.

## 1. Introduction

Robotic arms have become an essential aspect of every industry, with applications ranging from welding to component assembly or pick and place various objects. The proposed research explores the application of 6-DOF robotic manipulators with a cylindrical coordinate system-based workspace on uncrewed, off-road and extraterrestrial exploration vehicles referred to as "UGVs". The cylindrical type of arm can be designed with various configurations, namely, PPR, PRP and RPP. The PRP configuration to design our arm. By putting the revolute joint after the first prismatic, we eliminate the load of the first prismatic on the revolute joint. Although the PPR configuration has similar advantages as the PRP type, it falls short when it comes to its workspace, which is smaller than PRP. The cylindrical arm offers several advantages over the standard articulated or SCARA type arms. The use of 2 prismatic joints in the cylindrical arm allows individual axes to be controlled separately. For example, tasks that require the end effector to follow a straight line can be performed easily. The use of rotary joints in the articulated and SCARA type arm causes each link to move in two axes simultaneously, increasing the difficulty in the controllability of the arm.

Fikrul Akbar Alamsyah in [1] illustrates the use of a RPP type 3-dof cylindrical manipulator for fused filament fabrication (FFF) 3D printing. Global axis frames are established using the D-H method to solve kinematic problems to simulate the cylindrical arm as a FFF 3D printer. In [2] Billing et al. describe the development of NASA-JPL's Curiosity Rover's rugged robotic arm equipped with 5 turret-mounted scientific analysis instruments weighing 37 kgs.

In [3] Chaturvedi designed 3-DOF robotic arms using a CAD software, CATIA V5 and analyses (Static, modular and fatigue analysis) them with three different materials which are AISI-1050 steel, carbon fibre and kevlar-29.

Kannan et al. in [4] use ANSYS Workbench 18.0 AC Pre and Post to analyse and optimise the design of a hybrid aluminum - prepreg carbon fibre and epoxy composite drive shaft. Narayan et al. [5] presented the CAD and CAE based design of a 5 DOF manipulator

* Corresponding author.
*E-mail address:* atirav200129@gmail.com (A. Seth).

https://doi.org/10.1016/j.matpr.2022.02.365
2214-7853/
Selection and peer-review under responsibility of the scientific committee of the International Conference on Recent Advances in Modeling and Simulations Techniques in Engineering and Science.

equipped with a three-jaw gripper, to be utilized to automate physiotherapy procedures. The authors of [6] utilize industry-grade software's, SOLIDWORKS and ANSYS workbench for the iterative design and dynamic finite-element analysis respectively, of a 3-DOF robotic manipulator. Sai Santosh [7] performs finite element analysis using ANSYS workbench with ABS and PLA to compare structures, determine failure point and perform topology optimization to save material. In [8] Shanmugasundar et al. illustrate a comprehensive set of design procedures to be followed at for the development of a robotic manipulator, the authors utilize topological optimization tools on FEM software (ANSYS Workbench) to enhance the stiffness to weight performance of the links. In [9], Wang analyses all configurational permutations of 6-DOF manipulators comprising only of turning and sliding pairs and derives the configurations that are known as Cartesian, Cylindrical, Spherical, Articulated and Double cylindrical robots. Zhang et al. [10] explored the kinematics, dynamics and FEA based design of a 3-DOF manipulator featuring two translational and one rotational degree of freedom, to be utilized for pick and place operations in the post-processing of powder metallurgic parts. The robotic manipulator described by the authors of [11] features a lightweight variable configuration arm design and high precision actuating parts, that provide considerable advantage over conventional manipulators used in space applications. The authors of [12] review design and applications of state-of-the-art of tensegrity structures-based robots. R. Bonitz et al. in [13] describe the design of the articulated robotic arm present on board the Phoenix Mars Lander. Bloch et al. in [14] compare three different configurations of a 3-degree of freedom manipulator (RRR, PRR and PPP) and compares them for optimal harvesting of apples in an orchid. R. Oberti in [15] proposes a 6 DOF arm designed for automatic detection and selective spraying of grapevine canopy areas exhibiting symptoms of powdery mildew. In [16], A.Roshanianfard et al. present a design for a 4- degrees of freedom robotic manipulator which can be used for harvesting heavy crops such as melons and pumpkins in an outdoor agricultural environment. The Instrument Deployment Device (IDD) design, which is the 5 DOF manipulator on NASA's twin geological survey rovers, Spirit and Opportunity, is described by the authors of [17].

The aim is to make the manipulator able to take frontal head-on collision loads, while keeping the deformation within the elastic range while also keeping the weight of the manipulator low. This paper analyses the mechanical design of a 3-DOF cylindrical manipulator with a PRP joint configuration and a 3-DOF wrist. The arm has a vertical reach of 1.2 m and a horizontal reach of 0.8 m and can be mounted on a UGV, which is supposed to traverse off-road terrain, carry a payload of 5Kgs and perform dexterous operations. This paper primarily focuses on the structural components' rigidity of the robotic arm since the UGV maneuvers over rugged terrain; thus, high inertial loads and high-velocity collisions are expected. FE analysis is done on the structures using ANSYS workbench (Ver 19.2) and was modelled using SOLIDWORKS (Ver. 2019). Structures with high rigidity, such as wire bracings and composite materials such as carbon fibre, have been used to ensure a smooth operation of the tasks. The robotic manipulator can be used in rugged and demanding environments that require manipulation and servicing of high precision.

## 2. Robot description

The manipulator is divided into two sections, the robotic arm and the end effector, comprising 3 DOFs each. The robotic arm discussed in this paper is of PRP configuration, consisting of 2 translational DOFs and one rotational DOF for positioning of the manipulator. The wrist consists of 2 rotational DOFs for orientation

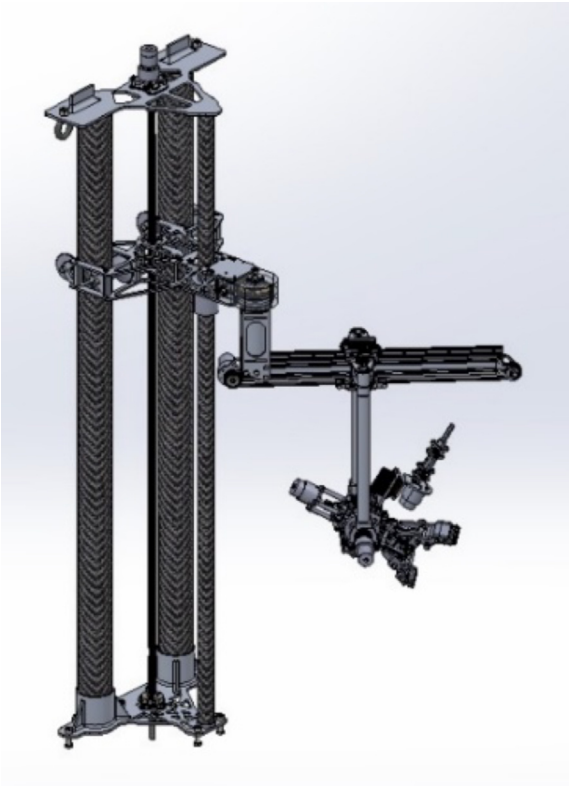

**Fig. 1.** 6-DOF Cylindrical Robotic Manipulator.

and a single DOF of the gripping mechanism (Fig. 1). The guide rod structure consists of three Roll-Wrapped Carbon fibre tubes. These tubes are mounted in a triangular pattern, which provides an adequate second moment of area for forward collisions. The two larger hind tubes have an outer diameter of 63 mm and a thickness of 1.5 mm, and the smaller fore tube has an outer diameter of 30 mm and a thickness of 2.5 mm. To provide additional rigidity to the first prismatic structure, reinforcement Guy wires are used to support the tall cantilevered first prismatic and are attached from the top plate to the mounting surface (chassis), tensioned using a turnbuckle.

The carriage assembly is a space frame structure that consists of Aluminum 6061-T6 topology-optimised plates that are bolted together. The rollers, which are an alternative to linear bearings, are manufactured by turning a solid nylon billet and only weighs 45g per roller, and each roller has a 130-degree contact arc, thus giving 260 degrees of total arc contact. Two lead nuts have been utilized, one mounted on each of the top and bottom plates, ensuring that both the plates have equal load distribution of the actuation forces. The Revolute joint in the manipulator connects the overhang and the first prismatic carriage. The revolute joint is driven by a Worm and worm wheel gearbox, which has a 40:1 reduction ratio. The gearbox is intrinsically non-back drivable, which helps self-lock the revolute joint when the motor is unpowered. The worm gearbox contains the bearing assembly for the revolute joint, and the gearbox casing is structurally analysed for taking collision and loading forces.

The overhang is a structural part of the arm used to mate the gearbox to the second prismatic structure. Such a structure was required to help extend the arm below the mounting surface. It makes use of a system consisting of Al 6061-T6 plates and a central tubular structure.

**Table 1**
Material Properties.

| Material | Density (kg m$^{-3}$) | Tensile Yield Strength (MPa) | Poisson's Ratio | Young's Modulus (GPa) |
|---|---|---|---|---|
| Aluminum 6061-T6 | 2,770 | 280 | 0.33 | 68 |
| Stainless Steel | 7,850 | 250 | 0.3 | 190 |
| Carbon fibre | 1,480 | 829 (X & Y) | 0.3 | 91.8 |

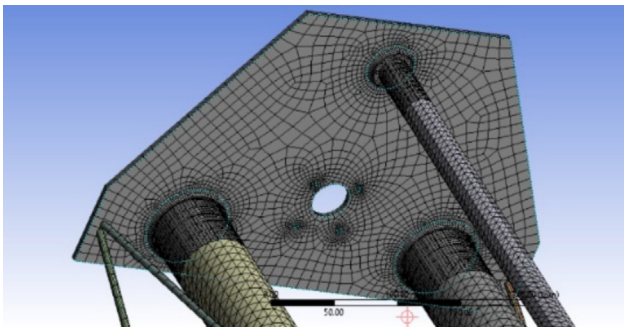

**Fig. 2.** Final meshing of the geometry for the analysis.

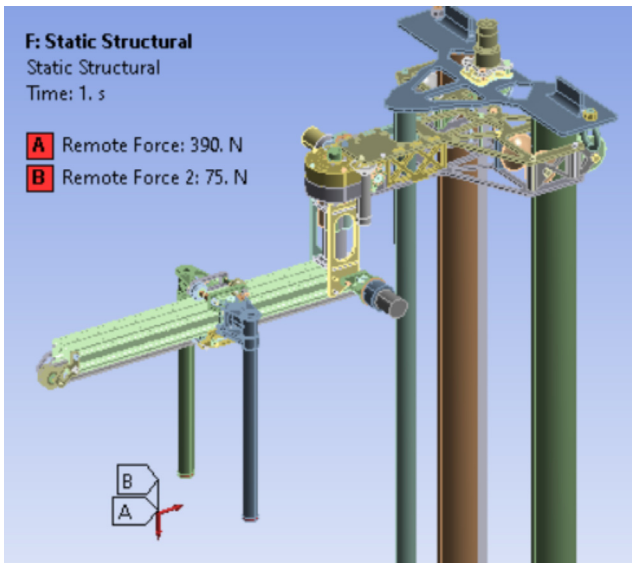


**Fig. 3.** Loading conditions.

## 3. Structural analysis using FEM

### 3.1. Material Properties

The materials considered for design and analysis are in Table 1.

### 3.2. Meshing

In Fig. 2 shows, the top milled connector, a Hexa/Prism mesh using multizone method with a size of 2 mm is used. The multizone mesh has a quadratic element order and four manual sources for mesh uniformity. The guy wires are meshed using sweep method with quadratic elements which have 100 elements, and the tubes were meshed using a uniform surface meshing before applying the ply using AC Pre.

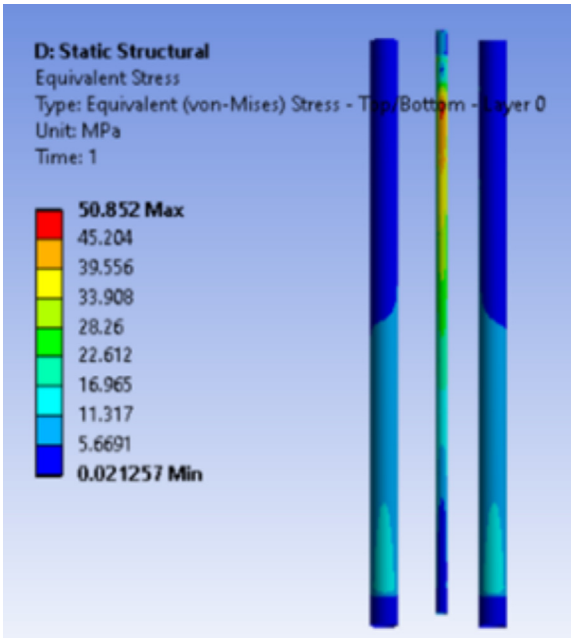


**Fig. 4.** (a-b). Maximum stress and strain distribution.

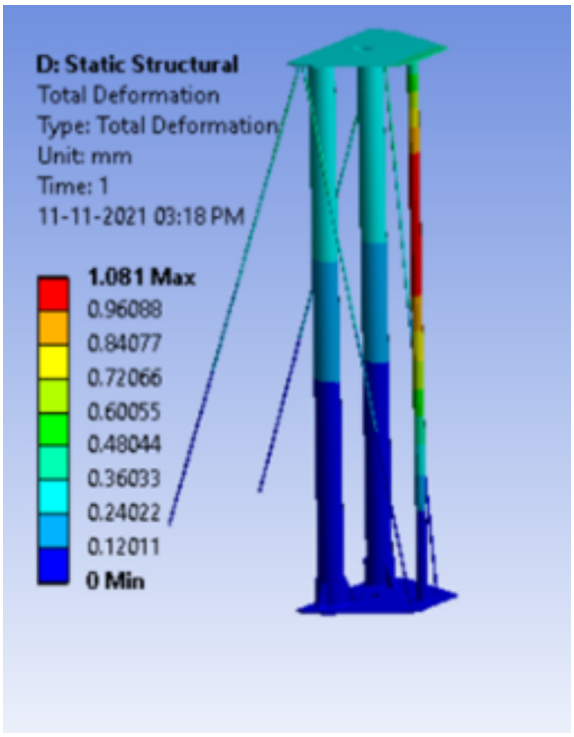


**Fig. 4** (*continued*)

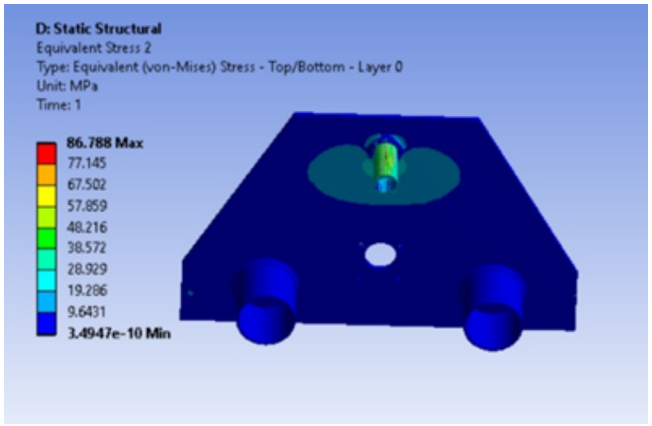


**Fig. 4** (*continued*)

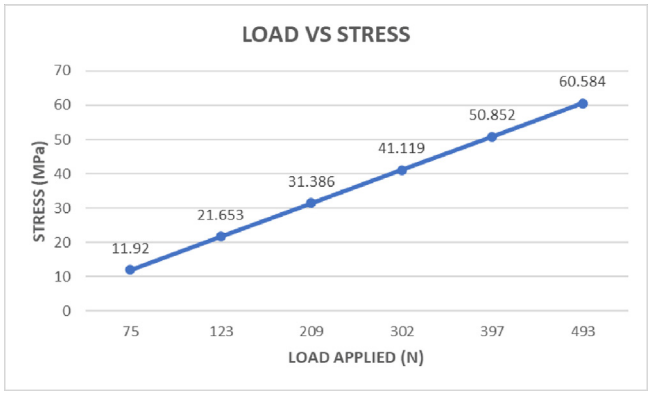


**Fig. 5** (*continued*)

### 3.3. Loading conditions

As show in Fig. 3, the major test case where the forces were maximum is taken, which is when the UGV faces a head-on collision at a speed of 1.6 m/s and the arm faces a direct impact at the end effector. There are two major forces acting on any structural component which are due to the payload and the impulsive loads due to the collision. The collision force was calculated to be 390 N. In Fig. 3., The Remote load "A" is to simulate the Head-on collision force, which is 390 N, and Remote load "B" is to signify the mass load of the end effector(25 N), plus the Payload(50 N), resulting in a total load of 75 N.

## 4. Results and discussion

It is observed that maximum stress and strain occurs in the member sensitive to the respective direction of load application.

The magnitude of the maximum total deformation at the first prismatic joint is 0.858 mm and the maximum stress on the tubes is 50.852 MPa and on the aluminum connectors is 37.57 MPa (Fig. 4 (a-c).) According to the Tsai-Wu and Tsai-Hill criteria, the values are 0.082146 and 0.079917 respectively which is well below 1. The overhang structure (I) is connected directly to the revolute joint output, and it supports the rest of the arm. The maximum deformation is 0.3689 mm and the maximum stress is 148.86 MPa. The maximum deformation one the Overhang (II) is 3.2982 mm and the maximum stress is 194.5 MPa, which is on a part that is milled out of aluminum 7075 alloy. The Worm gearbox that actuates and supports the revolute joint has a maximum deformation of 0.0463 mm and a maximum stress of 55.667 MPa. The Fig. 5 (a-b) shows the carbon fibre-based first

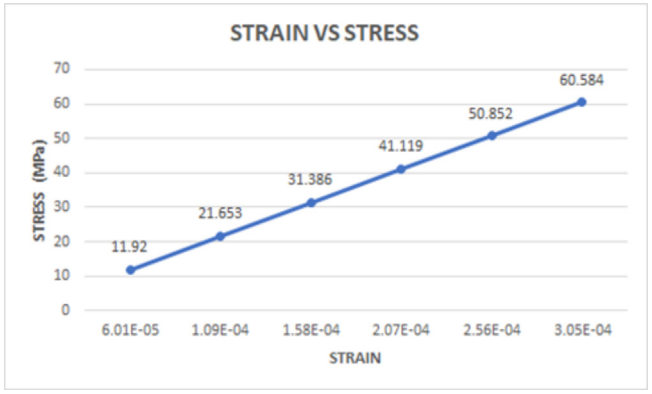


**Fig. 5.** (a-b) Distribution of Stresses due the various loading condition.

prismatic structure is analysed for various loading conditions, ranging from 0 collision force to 125% of the collision force (493 N). The various cases were 0, 25%, 50%, 75%, 100% and 125% of collision force, paired with the constant mass load of the payload and end effector (75 N). It is observed that the load v/s deformation (Fig. 5 (a)) and the stress v/s strain (Fig: 5. (b)), the behavior of graph is linear, which signifies the stress values are within the proportional limit, which is up to yield point of the material.

Hence, the deflections are elastic in nature.

## 5. Conclusion

This research includes a 6 degree Freedom cylindrical manipulator constructed to be equipped along with a UGV. The design is done while keeping in mind that the robotic manipulator should be robust to meet harsh load conditions while performing deft tasks. The main objective of this study is on structural analysis of the prismatic structure due to the design challenges faced with a large cantilever that increases the moment it acts during frontal collisions and other loading conditions. This requires that the structure has a high ratio of stiffness to weight. After iterative analysis of various tube configurations, layouts and tube dimensions, the three carbon fiber tubes used in a triangular arrangement proved rigid because the triangles are inherently more structurally robust than other arrangements. A steel wire support system is also implemented, which redistributes most of the stress caused by the force of impact during collisions.

The proposed structure can withstand a cantilever load, in the range of 75 N (static loading due to payload only) to 493 N (static loading along with 125% of the Collision force), while remaining within the elastic proportionality limit. The maximum deformation found in the structural analysis was 4 mm.

## Declaration of Competing Interest

The authors declare that they have no known competing financial interests or personal relationships that could have appeared to influence the work reported in this paper.

## References

[1] Alamsyah, F. A. The kinematics analysis of robotic arm manipulators cylindrical robot rpp type for fff 3d print using scilab. In IOP Conference Series: Materials Science and Engineering (2019), vol. 494, IOP Publishing, p. 012100.

[2] Billing, R., and Fleischner, R. Mars science laboratory robotic arm. In 14th European Space Mechanisms & Tribology Symposium, Constance, Germany, Sept (2011), pp. 28–30.

[3] R. Chaturvedi, A. Islam, K. Sharma, Anticipated investigation of a cylindrical robot arm by means of compound materials, European J. Mol. Clinical Med. 7 (4) (2020) 736–745.
[4] Kannan, V., Kannan, V. V., and Pemmasani, S. Design optimization of an epoxy carbon prepreg drive shaft and design of a hybrid aluminium 6061-t6 alloy/ epoxy carbon prepreg drive shaft. Tech. rep., SAE Technical Paper, 2018.
[5] J. Narayan, S. Mishra, G. Jaiswal, S.K. Dwivedy, Novel design and kinematic analysis of a 5-dofs robotic arm with three-fingered gripper for physical therapy, Mater. Today: Proc. 28 (2020) 2121–2132.
[6] A. Roy, T. Ghosh, R. Mishra, S.S. Kamlesh, Dynamic fea analysis and optimization of a robotic arm for ct image guided procedures, Mater. Today: Proc. 5 (9) (2018) 19270–19276.
[7] L.P.S. Santosh, N. Mishra, S.S.A. Mahanta, V. Dharmarajan, S.K. Varma, S. Shoor, Design and analysis of a robotic arm under different loading conditions using fea simulation, Mater. Today: Proc. (2021).
[8] G. Shanmugasundar, R. Sivaramakrishnan, S. Meganathan, S. Balasubramani, Structural optimization of an five degrees of freedom (t-3r-t) robot manipultor using finite element analysis, Mater. Today: Proc. 16 (2019) 1325–1332.
[9] K. Wang, T.K. Lien, Structure design and kinematics of a robot manipulator, Robotica 6 (4) (1988) 299–309.
[10] L. Zhang, X. Yan, Q. Zhang, Design and analysis of 3-dof cylindrical-coordinate based manipulator, Rob. Comput. Integr. Manuf. 52 (2018) 35–45.
[11] N. Sreekanth, A. Dinesan, A.R. Nair, G. Udupa, V. Tirumaladass, Design of robotic manipulator for space applications, Mater. Today: Proc. 46 (2021) 4962–4970.
[12] Y. Liu, Q. Bi, X. Yue, J. Wu, B. Yang, Y. Li, A review on tensegrity structures-based robots, Mech. Mach. Theory 168 (2022) 104571, https://doi.org/10.1016/j.mechmachtheory.2021.104571.
[13] Bonitz, R., Shiraishi, L., Robinson, M., Carsten, J., Volpe, R., Trebi-Ollennu, A., Arvidson, R. E., Chu, P., Wilson, J., and Davis, K. The phoenix mars lander robotic arm. In 2009 IEEE Aerospace conference (2009), IEEE, pp. 1–12.
[14] V. Bloch, A. Degani, A. Bechar, A methodology of orchard architecture design for an optimal harvesting robot, Biosyst. Eng. 166 (2018) 126–137.
[15] R. Oberti, M. Marchi, P. Tirelli, A. Calcante, M. Iriti, M. Hočevar, J. Baur, J. Pfaff, C. Schütz, H. Ulbrich, Selective spraying of grapevine's diseases by a modular agricultural robot, J. agricultural Eng. 44 (2s) (2013), https://doi.org/10.4081/jae.2013.271.
[16] A. Roshanianfard, N. Noguchi, T. Kamata, Design and performance of a robotic arm for farm use, Int. J. Agric. Biol. Eng. 12 (1) (2019) 146–158.
[17] Trebi-Ollennu, A., Baumgartner, E. T., Leger, P. C., and Bonitz, R. G. Robotic arm in-situ operations for the mars exploration rovers surface mission. In 2005 IEEE International Conference on Systems, Man and Cybernetics (2005), vol. 2, IEEE, pp. 1799–1806.